Bond charge depletion, bond strength and the impact sensitivity of high energetic 1,3,5-triamino 2,4,6-trinitrobenzene (TATB) molecule: A theoretical charge density analysis

ARTICLE *in* COMPUTATIONAL AND THEORETICAL CHEMISTRY · APRIL 2009

Impact Factor: 1.55 · DOI: 10.1016/j.comptc.2011.04.026

3 AUTHORS, INCLUDING:

Dr. Srinivasan Ponnusamy
C. Kandaswami Naidu College for Men, Che…
10 PUBLICATIONS **38** CITATIONS
SEE PROFILE

Poomani Kumaradhas
Periyar University
82 PUBLICATIONS **288** CITATIONS
SEE PROFILE

Computational and Theoretical Chemistry 967 (2011) 250–256

Contents lists available at ScienceDirect

Computational and Theoretical Chemistry

journal homepage: www.elsevier.com/locate/comptc

Bond charge depletion, bond strength and the impact sensitivity of high energetic 1,3,5-triamino 2,4,6-trinitrobenzene (TATB) molecule: A theoretical charge density analysis

A. David Stephen, P. Srinivasan, P. Kumaradhas *

Department of Physics, Periyar University, Salem 636 011, India

ARTICLE INFO

Article history:
Received 11 April 2011
Accepted 19 April 2011
Available online 27 April 2011

Keywords:
Quantum chemical calculation
Charge density analysis
Bond charge depletion
Molecular electrostatic potential
Impact sensitivity

ABSTRACT

A charge density study on 1,3,5-triamino 2,4,6-trinitrobenzene (TATB) energetic molecule has been carried out using density functional (B3P86/6-311G**) method and AIM theory. The bond topological analysis predicts that the bond charges of nitro group attached C—NO_2 bonds are highly depleted, hence it is the weakest bond in the molecule; whereas in the amino group attached C—NH_2 bonds, the bond charges are found highly concentrated, confirm that these bonds are much stronger than C—NO_2 bonds. The isosurface of molecular electrostatic potential exhibit large electronegative regions near the nitro groups. The electrostatic potential at the mid points of C_{ar}—C_{ar} and C—NO_2 bonds is found highly positive and are the sensitive bonds in the molecule. The relationship between the bond charge depletion and the impact sensitivity reveals the sensitive bonding regions of the molecule.

1. Introduction

In modern ordnance, there are certain desirable requirements for explosives: they should possess good thermal stability, less impact and shock sensitivity. Today, the main goal of synthesizing the new energetic materials is, to have less sensitive materials to avoid accidental detonations [1]. The decomposition, sensitivity and stability of high energetic materials are largely rely upon the fundamental properties such as bond strength and electrostatic potential of the molecules. These properties can be determined from the charge density analysis of molecules, either experimental or theoretical methods. Evaluation of the above bond-related properties [2] such as electron density $\rho_{bcp}(r)$, the Laplacian of electron density $\nabla^2\rho_{bcp}(r)$ and the molecular electrostatic properties includes atomic charges, electrostatic potential, and dipole moments are indispensable. Among these, the Lapalcian of electron density plays a central role on identifying the regions of space, where the charges are locally concentrated or depleted [3]. The information obtained from charge density distribution allows predicting the strength of inter and intra-molecular bonds of the molecules [4–10]. Furthermore, there are reports showing the relation between the molecular electrostatic potential (ESP) and the impact sensitivity [11–13] of the energetic molecules. Specifically, Murray et al.'s hypothesis [13], allows estimating the impact sensitivity of explosives from the degree of internal charge separation and the presence of strong electrostatic potential maxima on the molecular surface. The titled molecule 1,3,5-triamino-2,4,6-trinitrobenzene (TATB) (Fig. 1) [14] is a high energetic explosive molecule. The crystal structure of this molecule exhibit a layered structure and forming strong inter and intramolecular hydrogen bonding interactions [15]. Relatively, TATB is an insensitive explosive material on compared with other explosives [16]. It is believed that the extraordinary stability of TATB under thermal, impact or shock initiation conditions result from its significant inter and intramolecular hydrogen bonding interactions [17]. Further, some of the gas phase (isolated molecule) studies on TATB molecule, reports, how the intra-molecular hydrogen bonding [18–20] interactions are responsible for its high stability and its unusual insensitivity towards external stimuli, etc. [21,22]. In the structural point of view, the crystal density of TATB is higher than RDX (cyclotrimethylenetrinitramine) [14] and its elemental composition (C, H, N, O) is also same as RDX. Moreover, its explosive performance for a given amount is more powerful than the equivalent amount of 2,4,6-trinitrotolune (TNT). Because of its safety characteristics and high stability, it is being used for the military and civil applications [23]. Hence, we have chosen TATB to understand its bond topological and the electrostatic properties and further to relate its bond charge depletion with the impact sensitivity.

Nowadays, Density Functional Theory (DFT) [24] calculations are being carried out largely to explore the electronic properties of the molecule. The charge density distribution of the molecules can be determined from the wave function using Bader's Theory of Atoms in Molecules (AIM) [4], which are very useful to understand the nature of chemical bonds, reactivity, and stability of molecular systems. Also, it provides the essential bond topological

* Corresponding author. Tel.: +91 (0)427 2345520; fax: +91 (0)427 2345565.
E-mail address: kumaradhas@yahoo.com (P. Kumaradhas).

2210-271X/$ - see front matter © 2011 Elsevier B.V. All rights reserved.
doi:10.1016/j.comptc.2011.04.026

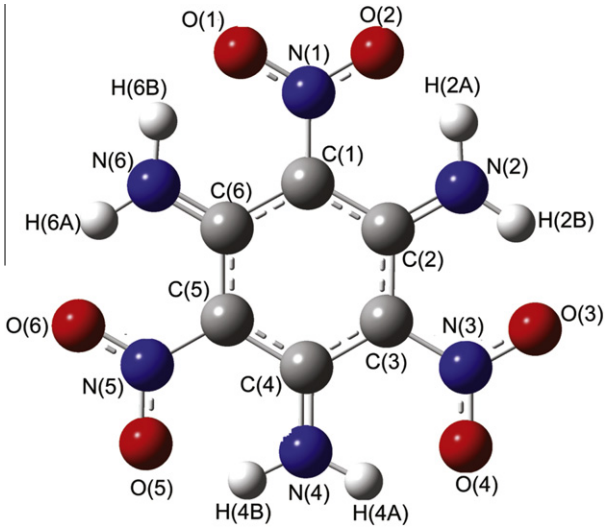

Fig. 1. Energy minimized molecular structure of TATB at B3P86/6-311G** level.

properties of the electron density $\rho_{bcp}(r)$ at the bond critical point, where $\nabla\rho(r) = 0$. The critical point of molecule can be classified according to its rank and signature [25]. The rank ω of critical point is equal to the number of non-zero eigen values of the Hessian matrix of $\rho_{bcp}(r)$ and the signature σ is the algebraic sum of the signs of the eigen values; the classification is written as (ω, σ). If the eigen values are positive, its associated eigenvector or gradient path (the path of the steepest ascent) originates at, and is directed away from the critical point. For negative eigenvalue the gradient path terminates at, and is directed towards the critical point. Among the four non-degenerate critical points; only the $(3, -1)$ type of bond critical points (bcp's) were considered in this study.

The Laplacian of electron density bear the chemical significance. If $\nabla^2\rho_{bcp}(r) < 0$, the charges are locally concentrated, the interaction is a *open-shell* type interaction and if $\nabla^2\rho_{bcp}(r) > 0$, the charges are locally depleted and the atomic interaction is a *closed-shell* type interaction. It is much more valid when the Laplacian of electron density is correlated with local total energy density $H(r)$ [26], which facilitates for the identification of strong and weak bonds in the molecule. The local total energy density is defined as

$$H(r) = [G(r) + V(r)] \quad (1)$$

where $G(r)$ is the local kinetic energy density and $V(r)$ is the local potential energy density in the bonding region. The dominance of $V(r)$ results negative $H(r)$ and the stabilization of the molecule; the destabilization results from the dominance of kinetic energy density [9].

2. Computational details

The optimization of TATB molecule (Fig. 1) has been carried out from the density functional method B3P86 [27] with the basis set 6-311G** using GAUSSIAN03 software [28]. The calculated molecular geometric parameters of TATB almost agree with the reported experimental geometry [15] except N—H bond distances, which are longer than the experimental values; this is attributed to the problem of locating H-atoms from the X-ray diffraction technique (Table 1). The intramolecular hydrogen bonding interactions are calculated and the bond parameters are presented in Table 2 along with the corresponding experimental values. The wave function obtained from the DFT calculation is used to compute the bond topological parameters such as; electron density, Laplacian of electron density and bond ellipticity, using AIMPAC software [29]. The integrated charges (AIM charges) are calculated using AIMALL software [30]. The programs *wfn2plots* and XD [31] are used to produce the deformation and the Lapalcian of electron density maps. The electrostatic potential of the molecule has been plotted with MOLISO software [32] to visualize the iso-surface of positive and negative ESP regions of the molecule.

Table 1
Selected geometric parameters (Å, °) from DFT and experimental [15] calculations.

Bonds	B3P86	Exp.
Bond lengths		
C(1)—C(2)	1.440	1.436
C(2)—C(3)	1.440	1.448
C(3)—C(4)	1.440	1.437
C(4)—C(5)	1.440	1.446
C(5)—C(6)	1.440	1.435
C(6)—C(1)	1.440	1.450
C(1)—N(1)	1.430	1.417
C(3)—N(3)	1.430	1.417
C(5)—N(5)	1.430	1.422
C(2)—N(2)	1.321	1.309
C(4)—N(4)	1.321	1.319
C(6)—N(6)	1.321	1.311
N(1)—O(1)	1.236	1.236
N(1)—O(2)	1.236	1.243
N(3)—O(3)	1.236	1.246
N(3)—O(4)	1.236	1.239
N(5)—O(5)	1.236	1.243
N(5)—O(6)	1.236	1.260
N(2)—H(2A)	1.016	0.865
N(2)—H(2B)	1.016	0.849
N(4)—H(4A)	1.016	0.757
N(4)—H(4B)	1.016	1.054
N(6)—H(6A)	1.016	0.868
N(6)—H(6B)	1.016	0.954
Bond angles		
C(1)—C(2)—C(3)	118.9	118.0
C(2)—C(3)—C(4)	121.1	121.8
C(3)—C(4)—C(5)	118.8	118.0
C(4)—C(5)—C(6)	121.0	122.3
C(5)—C(6)—C(1)	118.8	117.5
C(6)—C(1)—C(2)	121.1	122.2
C(2)—C(1)—N(1)	119.4	119.2
C(6)—C(1)—N(1)	119.4	118.6
C(2)—C(3)—N(3)	119.4	119.2
C(4)—C(3)—N(3)	119.4	119.1
C(4)—C(5)—N(5)	119.4	118.6
C(6)—C(5)—N(5)	119.4	119.1
C(1)—C(2)—N(2)	120.6	121.3
C(3)—C(2)—N(2)	120.4	120.7
C(3)—C(4)—N(4)	120.6	121.4
C(5)—C(4)—N(4)	120.5	120.6
C(5)—C(6)—N(6)	120.6	121.4
C(1)—C(6)—N(6)	120.5	121.1
C(1)—N(1)—O(1)	120.6	121.4
C(1)—N(1)—O(2)	120.6	120.7
C(3)—N(3)—O(3)	120.6	120.7
C(3)—N(3)—O(4)	120.6	121.5
C(5)—N(5)—O(5)	120.6	121.3
C(5)—N(5)—O(6)	120.6	121.2
N(1)—C(1)—C(2)—N(2)	2.4	2.6

Table 2
Intramolecular hydrogen bonding interactions (DFT/Exp.).

D—H···A	H···A(Å)	D···A(Å)	∠D—H···A (°)
N(2)—H(2A)···O(2)	1.680/1.797	2.492/2.497	133.6/136.0
N(2)—H(2B)···O(3)	1.680/1.838	2.492/2.482	133.8/131.6
N(4)—H(4A)···O(4)	1.680/1.948	2.492/2.508	133.6/130.6
N(4)—H(4B)···O(5)	1.680/1.692	2.492/2.478	133.7/127.6
N(6)—H(6A)···O(6)	1.680/1.816	2.492/2.505	133.7/134.4
N(6)—H(6B)···O(1)	1.680/1.770	2.492/2.486	133.7/129.9

3. Electron density distribution

Fig. 2, depicts the deformation density of the molecule calculated from the wave function obtained from DFT calculation. The deformation density map shows the aspherical nature of the electron density of atoms in molecules, which allows visualizing the areas of charge accumulation in the bonding regions and the lone pair positions of atoms in molecules. The deformation map of TATB molecule reveals the covalent nature of bonds from the continuous region of charge density distribution of the molecule. A complete spectrum of charge density distribution obtained from the bond topological analysis of TATB is presented in Table 3. Although the C—NO_2 bonds exhibit covalent interaction, its charge density distribution is not similar to the other bonding regions of the molecule; the map clearly differentiates the difference of charge density distribution of various bonding regions of the molecule. The electron density $\rho_{bcp}(r)$ at the bcp's of C_{ar}—C_{ar} bonding regions ($\sim$1.92 eÅ^{-3}) are considerably less when compared with the reported values ($\sim$2.1 eÅ^{-3}) of similar bonds [33–36]. The difference of $\rho_{bcp}(r)$ values among the bonds of the ring, reflect the effect of substituents (amino and nitro groups) in the ring. Similarly, the charge accumulation in the NO_2 group attached C—N bonds is also found less ($\sim$1.85 eÅ^{-3}) on compared with the amino group attached C—N bonds ($\sim$2.35 eÅ^{-3}). Notably, the charge accumulation in all N═O bonds ($\sim$3.29 eÅ^{-3}) are found high, which are the maximum charge density bearing bonds in the molecule. Comparatively, the charge accumulation ($\sim$1.92 and $\sim$1.85 eÅ^{-3}) and the bond order (1.2 and 1.1) [37] of C_{ar}—C_{ar} and C—NO_2 bonds are found to be less. The low values of $\rho_{bcp}(r)$ indicate that the charges of these bonds are not well localized in the bonding region. However, it requires more interpretation in terms of Laplacian of electron density.

The bond path analysis has been carried out to understand the bond charge polarization of each bond in the molecule; in which the C_{ar}—C_{ar} bonds are the less polarized bonds, which is confirmed from the small bcp shift of about less than 0.9%. But, the trend in the C—N bonds (C—NO_2 and C—NH_2) are found significantly different, i.e., the bcp positions of these bonds are shifted largely from the middle of the bonds at about 13%, towards the respective carbon atoms; this amount of shift indicates that the charges of these bonds are highly polarized. In the N═O bonds, the charges are slightly polarized towards the N-atoms and the bcp shift is 2.3%. Table 3, shows the complete spectrum of bond charge polarization of the molecule, in which, the C—NO_2 and N—H bonds are considered as the highly polarized bonds.

4. Laplacian of electron density and energy density

The Laplacian of electron density at the bcp [$\nabla^2\rho_{bcp}(r)$] provides significant information about the charge concentration/depletion of chemical bonds, which allows predicting the strength of bonds and the type of interaction exist between the atoms in molecule. Here, we have calculated $\nabla^2\rho_{bcp}(r)$ and the energy density distribution of each bond of the TATB molecule. Fig. 3, shows the Laplacian of electron density distribution in the molecular plane. In the N═O bonds, the electron density of O-atoms concentrates mainly in the non-bonding direction, which emphasizes the lone pair regions. In general, the contours of the C_{ar}—C_{ar} bonds of the aromatic ring shows a uniform charge distribution and the charges are used to be concentrated; whereas in the present study, the charges of C_{ar}—C_{ar} bonds of TATB molecule are considerably depleted on compared with the reported similar bonds [33–36,38–40]; its average $\nabla^2\rho_{bcp}(r)$ value is -17.6 eÅ^{-5}. This unusual large charge depletion may be due to the effect of nitro and amino groups present at the alternate positions of C-atoms of the ring. The DFT method predicts, the charges of nitro group attached C—N bonds are highly depleted, its corresponding Laplacian values are found considerably less (~-14.9 eÅ^{-5}) on compared with that of amino group attached C—N bonds, where the charges are highly concentrated

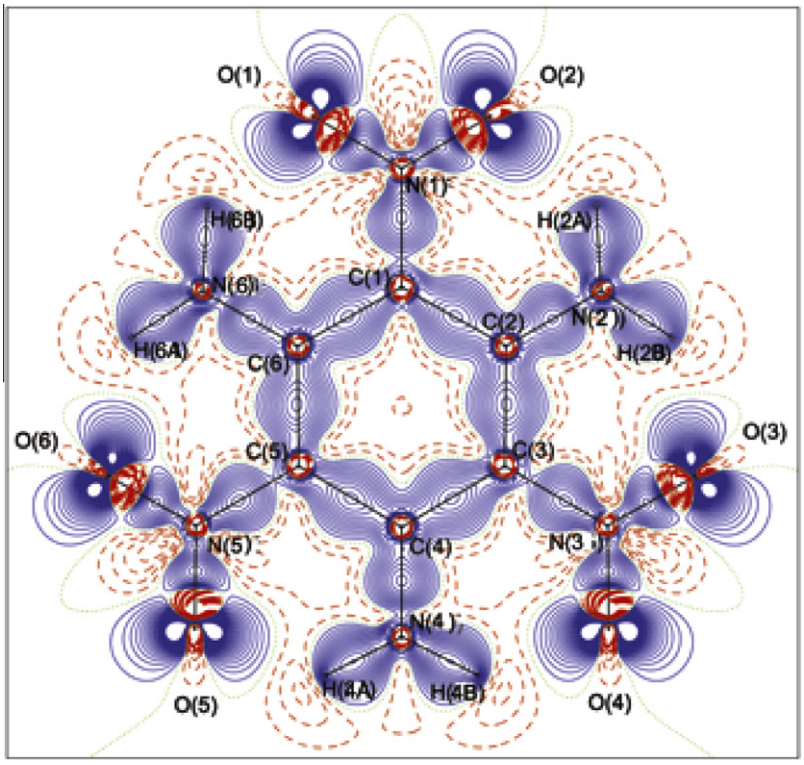

Fig. 2. Deformation density in the plane of the molecule. The solid lines (blue) are positive, dashed (red) are negative and dotted lines are zero contours. Contour intervals are drawn at 0.05 eÅ^{-3}. (For interpretation of the references to color in this figure legend, the reader is referred to the web version of this article.)

Table 3
Bond topological properties of TATB molecule.

Bonds	$\rho_{bcp}(r)$[a]	$\nabla^2\rho_{bcp}(r)$[b]	λ_1[c]	λ_2[c]	λ_3[c]	Bond order	ε[d]	d_1[e]	d_2[e]	D[f]	Δd%[g]
C(1)—C(2)	1.92	−17.6	−14.2	−11.5	8.1	1.2	0.24	0.707	0.733	1.440	0.9
C(2)—C(3)	1.92	−17.6	−14.2	−11.5	8.1	1.2	0.24	0.733	0.707	1.440	0.9
C(3)—C(4)	1.92	−17.6	−14.2	−11.5	8.1	1.2	0.24	0.707	0.733	1.440	0.9
C(4)—C(5)	1.92	−17.6	−14.2	−11.5	8.1	1.2	0.24	0.733	0.707	1.440	0.9
C(5)—C(6)	1.92	−17.6	−14.2	−11.5	8.1	1.2	0.24	0.707	0.733	1.440	0.9
C(6)—C(1)	1.92	−17.6	−14.2	−11.5	8.1	1.2	0.24	0.733	0.707	1.440	0.9
C(1)—N(1)	1.85	−14.9	−13.3	−9.4	7.8	1.1	0.42	0.516	0.914	1.430	13.9
C(3)—N(3)	1.85	−14.9	−13.3	−9.4	7.8	1.1	0.42	0.516	0.914	1.430	13.9
C(5)—N(5)	1.85	−14.9	−13.3	−9.4	7.8	1.1	0.42	0.516	0.914	1.430	13.9
C(2)—N(2)	2.35	−23.9	−18.4	−16.1	10.6	1.4	0.14	0.488	0.833	1.321	13.0
C(4)—N(4)	2.35	−23.9	−18.4	−16.1	10.6	1.4	0.14	0.488	0.833	1.321	13.0
C(6)—N(6)	2.35	−23.9	−18.4	−16.1	10.6	1.4	0.14	0.488	0.833	1.321	13.0
N(1)—O(1)	3.29	−24.1	−30.8	−27.8	34.5	1.4	0.11	0.589	0.647	1.236	2.3
N(1)—O(2)	3.29	−24.1	−30.9	−27.8	34.5	1.4	0.11	0.589	0.646	1.236	2.3
N(3)—O(3)	3.29	−24.1	−30.9	−27.8	34.5	1.4	0.11	0.589	0.647	1.236	2.3
N(3)—O(4)	3.29	−24.1	−30.9	−27.8	34.5	1.4	0.11	0.589	0.646	1.236	2.3
N(5)—O(5)	3.29	−24.1	−30.9	−27.8	34.5	1.4	0.11	0.589	0.646	1.236	2.3
N(5)—O(6)	3.29	−24.1	−30.9	−27.8	34.5	1.4	0.11	0.589	0.646	1.236	2.3
N(2)—H(2A)	2.23	−44.3	−32.1	−31.0	18.8	0.7	0.03	0.774	0.220	0.994	27.9
N(2)—H(2B)	2.23	−44.3	−32.1	−31.0	18.8	0.7	0.03	0.774	0.220	0.994	27.9
N(4)—H(4A)	2.23	−44.4	−32.1	−31.1	18.8	0.7	0.03	0.774	0.220	0.994	27.9
N(4)—H(4B)	2.23	−44.3	−32.1	−31.1	18.8	0.7	0.03	0.774	0.220	0.994	27.9
N(6)—H(6A)	2.23	−44.3	−32.1	−31.0	18.8	0.7	0.03	0.774	0.220	0.994	27.9
N(6)—H(6B)	2.23	−44.3	−32.1	−31.0	18.8	0.7	0.03	0.774	0.220	0.994	27.9

[a] Electron density (eÅ^{-3}).
[b] Laplacian of electron density (eÅ^{-5}).
[c] Hessian eigen values (eÅ^{-5}).
[d] Bond ellipticity.
[e] Distance between the critical point and respective bonded atomic nucleus (Å).
[f] Total bond path length (Å).
[g] Displacement of bond critical point from the bond midpoint (%).

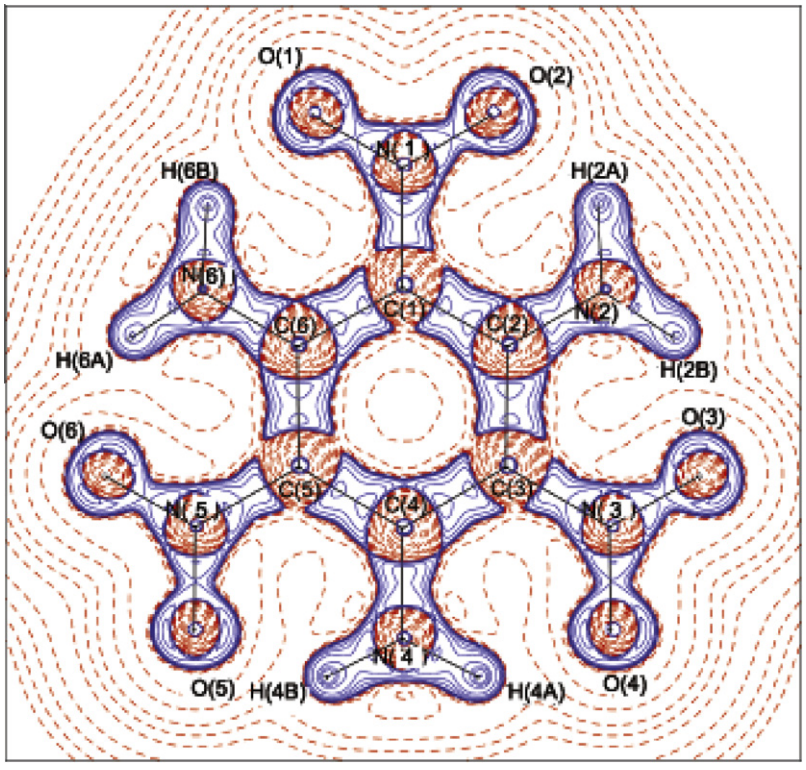

Fig. 3. Negative Laplacian of electron density $\nabla^2\rho(r)$ of TATB molecule. Contours are drawn on a logarithmic scale, 3.0×2^N eÅ^{-5}.

(∼−23.9 eÅ^{-5}). The difference of negative Laplacian $\nabla^2\rho_{bcp}(r)$ between the C—N bonds reveals that, the NO_2 groups are weakening the C—NO_2 bonds thereby depleting the bond charges; whereas the NH_2 groups are strengthening the C—NH_2 bonds. The Laplacian of N=O bonds (∼−24.1 eÅ^{-5}) are found highly negative, which indicates that the bond charges are moderately concentrated and

Table 4
Energy density distribution (HÅ^{-3}).

Bonds	$V(r)$	$G(r)$	$H(r)$
C(1)—C(2)	−2.36	0.56	−1.80
C(2)—C(3)	−2.36	0.56	−1.80
C(3)—C(4)	−2.36	0.56	−1.80
C(4)—C(5)	−2.36	0.56	−1.80
C(5)—C(6)	−2.36	0.56	−1.80
C(6)—C(1)	−2.36	0.56	−1.80
C(1)—N(1)	−3.78	1.37	−2.41
C(3)—N(3)	−3.78	1.37	−2.41
C(5)—N(5)	−3.78	1.37	−2.41
C(2)—N(2)	−5.18	1.75	−3.43
C(4)—N(4)	−5.17	1.75	−3.42
C(6)—N(6)	−5.18	1.75	−3.43
N(1)—O(1)	−6.52	2.42	−4.10
N(1)—O(2)	−6.53	2.42	−4.11
N(3)—O(3)	−6.53	2.42	−4.11
N(3)—O(4)	−6.53	2.42	−4.11
N(5)—O(5)	−6.53	2.42	−4.11
N(5)—O(6)	−6.53	2.42	−4.11
N(2)—H(2A)	−3.79	0.34	−3.45
N(2)—H(2B)	−3.79	0.34	−3.45
N(4)—H(4A)	−3.79	0.34	−3.45
N(4)—H(4B)	−3.79	0.34	−3.45
N(6)—H(6A)	−3.79	0.34	−3.45
N(6)—H(6B)	−3.79	0.34	−3.45

Table 5
Atomic charges (e).

Atoms	MPA	NPA	AIM
C(1)	0.19	−0.06	0.28
C(2)	0.20	0.26	0.62
C(3)	0.19	−0.06	0.28
C(4)	0.20	0.26	0.62
C(5)	0.20	−0.06	0.28
C(6)	0.20	0.26	0.62
O(1)	−0.34	−0.44	−0.50
O(2)	−0.34	−0.44	−0.50
O(3)	−0.34	−0.44	−0.50
O(4)	−0.34	−0.44	−0.50
O(5)	−0.34	−0.44	−0.50
O(6)	−0.34	−0.44	−0.50
N(1)	0.17	0.51	0.30
N(2)	−0.44	−0.68	−1.21
N(3)	0.17	0.51	0.30
N(4)	−0.44	−0.68	−1.21
N(5)	0.17	0.51	0.30
N(6)	−0.44	−0.68	−1.21
H(2A)	0.27	0.43	0.51
H(2B)	0.27	0.43	0.51
H(4A)	0.28	0.43	0.50
H(4B)	0.27	0.43	0.51
H(6A)	0.27	0.43	0.51
H(6B)	0.28	0.43	0.51

its corresponding potential energy density $V(r)$ is also found high (∼−6.53 HÅ^{-3}). Relatively, the charge concentration in N—H bonds is very high (∼−44.3 eÅ^{-5}), the same trend noticed in the reported structures [41–43]. Notably, the kinetic energy density $G(r)$ of these bonds is very low (∼0.34 HÅ^{-3}) on compared with all other bonds in the molecule (Table 4). Thus, from the investigation of Laplacian of electron density distribution of TATB molecule reveals that the charges of C_{ar}—C_{ar} and C—NO_2 bonds are significantly depleted on compared with all other bonds. Further, these bonds exhibit, very low local total energy density $H(r)$ [∼−1.80 and ∼−2.41 HÅ^{-3}]; this also confirm the existence of high charge depletion of these bonds. Hence, these two bonds are the weakest bonds in the molecule.

The spherical and aspherical nature of electron density at the bond critical points in the bonding region can be interpreted in terms of bond ellipticity [25], which is the ratio of eigen values λ_1 and λ_2 i.e., $\varepsilon = (\lambda_1/\lambda_2) - 1$. The high value of ellipticity shows the large anisotropy of electron density distribution in the bonding region. The maximum bond charge anisotropy is noticed in the high charge depleted C_{ar}—C_{ar} and C—NO_2 bonds, the respective ε-values are ∼0.24 and ∼0.42. The ε-values of all other bonds are found consistently much smaller (Table 3), which confirm that, the charges are almost isotropic.

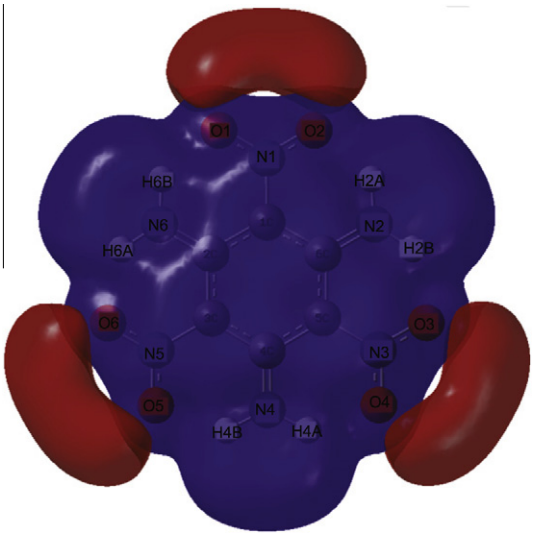

Fig. 4. Isosurface representation of electrostatic potential. Blue: positive potential (0.5 eÅ^{-3}), Red: negative potential (−0.5 eÅ^{-3}) and Green: zero potential. (For interpretation of the references to color in this figure legend, the reader is referred to the web version of this article.)

5. Atomic charges and electrostatic potential

The knowledge of charge distribution of the molecule is very much essential to understand the chemical reactivity, molecular electrostatic potential and the electrostatic interactions [44,45]. To explore the ESP of the molecule, here, we report three kinds

Table 6
Electrostatic potential at the bond mid points V_{mid} (eÅ^{-1}).

Bonds	MPA	NPA
C(1)—C(2)	0.55	0.28
C(2)—C(3)	0.55	0.28
C(3)—C(4)	0.55	0.28
C(4)—C(5)	0.56	0.28
C(5)—C(6)	0.56	0.28
C(6)—C(1)	0.55	0.28
C(1)—N(1)	0.50	0.62
C(3)—N(3)	0.50	0.62
C(5)—N(5)	0.51	0.62
C(2)—N(2)	−0.36	−0.64
C(4)—N(4)	−0.35	−0.64
C(6)—N(6)	−0.35	−0.64
N(1)—O(1)	−0.28	0.11
N(1)—O(2)	−0.28	0.11
N(3)—O(3)	−0.28	0.11
N(3)—O(4)	−0.28	0.11
N(5)—O(5)	−0.28	0.11
N(5)—O(6)	−0.28	0.11
N(2)—H(2A)	0.13	−0.50
N(2)—H(2B)	0.13	−0.50
N(4)—H(4A)	0.13	−0.51
N(4)—H(4B)	0.13	−0.51
N(6)—H(6A)	0.13	−0.50
N(6)—H(6B)	0.13	−0.50

of charges, which are obtained from Mulliken population analysis (MPA) [46], Natural Population Analysis (NPA) [47] and the Theory of Atoms in Molecules (AIM). The MPA and NPA charges are calculated from the method given in [46,47], which are implemented in Gaussian03 software [28]; whereas the AIM charges are from aspherical or multipole atom model [48]. The AIM scheme was developed by Bader and his coworkers [48], in which, the molecular charge density is divided into atomic contributions based on its overall topology. The charges calculated from these methods are presented in Table 5. Relatively, the AIM charges are consistently higher than the MPA and NPA models charges.

The AIM charges of C(1), C(3) and C(5) (NO_2 group attached) are found positive (∼0.28e), whereas the corresponding MPA and NPA charges are found less positive (∼0.19 and ∼−0.06e); the difference between these two model charges are may be due to different method of atomic charge estimation in the molecule. The average charge of amino group attached C-atoms [C(2), C(4), and C(6)] are positive ∼0.20 (MPA), ∼0.26 (NPA) and ∼0.62e (AIM), while the nitrogen atoms are carrying high negative charges, and the values are ∼−0.44 (MPA), ∼−0.68 (NPA) and ∼−1.21e (AIM). The net —NO_2 group charges are calculated from MPA/NPA/AIM models and the values are −0.51/−0.37/0.70e respectively. The difference of charge between C and N atoms of C—NO_2 bonds implies that these bonds are highly polarized; presumably, the bond charge polarization partly weakening the bond. The isosurface representation of ESP (Fig. 4) shows the large negative ESP surface is found near NO_2 regions, which indicate the negative charge domination of NO_2 groups.

6. Bond dissociation energy and impact sensitivity

The bond topological analysis predicts that the C—NO_2 and C_{ar}—C_{ar} bonds are the weak bonds in the molecule. To validate this, we have calculated bond dissociation energy (BDE) [49–52] for these bonds. The calculated BDE of C—NO_2, C_{ar}—C_{ar} and C—NH_2 bonds are 76.8, 104.7, 118.9 kcal/mol respectively; in which, the C—NO_2 bond exhibit lowest energy, it confirms that the nitro group attached C—N bond is the weakest bond in the molecule. Further, the BDE of C—NO_2 bond is also compared with the C—NO_2 bonds (70.1 kcal/mol) of TNB molecule [53]. Relatively, the BDE of TATB is slightly higher than the TNB molecule. The increase of BDE in TATB may be attributed to the non-bonding interaction of NO_2 with the adjacent NH_2 groups in the molecule, such interaction is not exist in TNB molecule.

On the basis of Murray et al's hypothesis [13], we have investigated the electrostatic potential at the bond mid points [54] defined as

$$V_{\text{mid}} = (q_i + q_j)/0.5R \tag{2}$$

where q_i and q_j are the atomic charges of the ith and jth atoms and R is the bond distance. Among the calculated V_{mid} values (Table 6), the C_{ar}—C_{ar} and C—NO_2 bonds exhibit high positive values (MPA: 0.55/0.50 and NPA: 0.28/0.62 e/Å). This positive potential implies the high bond charge depletion [55]. Fig. 5, shows the relationship between the bond charge depletion $\nabla^2\rho_{\text{bcp}}(r)$ and the impact sensitivity (V_{mid}) of each bond in the molecule. To accentuate this relationship, we have compared our recent finding (Table 7), which

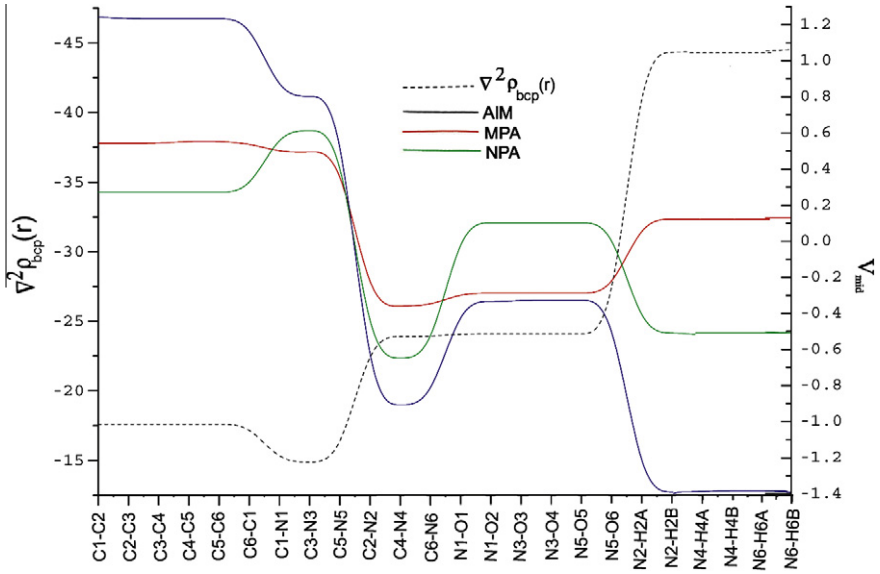

Fig. 5. Showing the relationship between Laplacian of electron density $\nabla^2\rho_{\text{bcp}}(r)$ and impact sensitivity V_{mid} of all bonds.

Table 7
Relationship between Laplacian of electron density $\nabla^2\rho_{\text{bcp}}(r)$ (eÅ^{-5}) with impact sensitivity V_{mid}, (eÅ^{-1}) of some nitro aromatic explosives.

Bonds	TATB		TNB [56]		TNT [57]		TNTA [58]	
	V_{mid}	$\nabla^2\rho(r)$	V_{mid}	$\nabla^2\rho(r)$	V_{mid}	$\nabla^2\rho(r)$	V_{mid}	$\nabla^2\rho(r)$
$(C—C)_{ar}$	0.28	−17.6	−0.13	−21.6	−0.48	−21.5	–	–
$(C—N)_{ar}$	–	–	–	–	–	–	0.16	−24.5
C—NO_2	0.62	−14.9	0.80	−16.7	0.81	−17.1	1.34	−14.5
C—NH_2	−0.64	−23.9	–	–	–	–	–	–
N—O(nitro)	0.11	−24.1	0.27	−27.3	0.29	−27.6	0.29	−22.7
N—H(amine)	−0.50	−44.3	–	–	–		–	–
$(C—H)_{ar}$	–	–	0.23	−24.8	0.14	−23.9	–	–

includes the relationship between V_{mid} and $\nabla^2\rho_{bcp}(r)$ of some nitro aromatic explosives [56–58]. The scenario in TATB comprises, the high charge depleted C_{ar}—C_{ar} and C—NO_2 bonds are the sensitive bonds in the molecule. The sensitivity of the molecule may be related to the presence of NO_2 groups in the molecular frame work. As the NO_2 groups added to the molecular framework, the attached bond (C—NO_2) become weaker, create an electrostatic imbalance in the molecule [55]. According to Murray et al., [55] the balance parameter ν reaches a maximum value 0.25, when $\sigma_+^2 = \sigma_-^2$. Here, we have calculated the positive and negative electrostatic potential variances (σ_+^2 and σ_-^2) and the electrostatic balance parameter (ν) [59,60] of TATB, the corresponding values are $\sigma_+^2 = 48.83, \sigma_-^2 = 59.57$ (kcal/mole^{-1})^2 and $\nu = 0.247$ respectively. The balance parameter is consistent with the reported insensitive energetic molecules [55]; confirm that TATB is a less sensitive molecule.

7. Conclusions

The present study on TATB explosive molecule is carried out to understand its bond topological, energetic and electrostatic properties, and further to relate its bond charge depletion with the impact sensitivity. From the bond topological properties and the energy density distribution, it confirms that the nitro group attached C—N bonds are the weakest bond in the molecule. A similar kind of investigation was carried out on aromatic C_{ar}—C_{ar} bonds, reveals that these bonds are also notably weak. Further, the impact sensitivity calculation (V_{mid}) predicts, the C_{ar}—C_{ar} and C—NO_2 bonds are more sensitive than the other bonds in the molecule. Above all, it can be concluded that these two bonds are the weakest bonds in the molecule, hence, it is expected that these bonds may rupture first, when the TATB material expose to external stimuli.

References

[1] P. Politzer, J.S. Murray, Energetic Materials Part 2 Detonation, Combustion, Elsevier, The Netherlands, 2003.
[2] M.A. Speckman, Chem. Rev. 92 (1992) 1769.
[3] R.F.W. Bader, Acc. Chem. Res. 18 (1985) 9.
[4] R.F.W. Bader, Atoms in Molecules-A Quantum Theory, Oxford University Press, Oxford, 1990.
[5] C.R. Lee, L.Y. Tan, Y. Wang, J. Phys. Chem. Solids 62 (2001) 1613.
[6] C.R. Lee, T.H. Tang, L. Chen, C.C. Wang, Y. Wang, J. Phys. Chem. Solids 65 (2004) 1957.
[7] R.F.W. Bader, T. Slee, D. Cremer, E. Kraka, J. Am. Chem. Soc. 105 (1983) 5061.
[8] R.F.W. Bader, T.H. Tang, Y. Tal, F.W. Biegler-König, J. Am. Chem. Soc. 104 (1982) 946.
[9] P. Cramer, E. Kraka, Croat.Chem. Acta 57 (1984) 1259.
[10] E. Espinosa, E. Molins, C. Lecomte, Chem. Phys. Lett. 285 (1998) 170.
[11] B.M. Rice, J.J. Hare, J. Phys. Chem. A 106 (2002) 1770.
[12] S. Zeman, Struct. Bond. 125 (2007) 195.
[13] J.S. Murray, P. Lane, P. Politzer, Mol. Phys. 85 (1995) 1.
[14] J. Akhavan, The Chemistry of Explosives, The Royal Society of Chemistry, UK, 2004.
[15] H.H. Cady, A.C. Larson, Acta. Crystallogr. 18 (1965) 485.
[16] S.F Rice, R.L. Simpson, Lawrence Livermore National Laboratory, Livermore, CA, Report UCRL-LR-103683, 1990.
[17] S. Roszak, R.H. Gee, K. Balasubramanian, L.E. Fried, Chem. Phys. Lett. 374 (2003) 286.
[18] B.M. Dobratz, Los Alamos National Laboratory, Los Alamos, NM, 1995.
[19] C.J. Wu, L.E. Fried, J. Phys. Chem. A104 (2000) 6447.
[20] M.R. Manaa, L.E. Fried, J. Phys. Chem. A105 (2001) 6765.
[21] K.L. McNesby, C.S. Coffey, J. Phys. Chem. B101 (1997) 3097.
[22] J. Sharma, B.C. Beard, M. Chaykovsky, J. Phys. Chem. 95 (1991) 1209.
[23] M.B. Talawar, A.P. Agarwal, M. Anniyappan, G.M. Gore, S.N. Asthana, S. Venugopalan, J. Hazard. Mater. B137 (2006) 1848.
[24] J.K. Labanowski, J.W. Andzelm, Density Functional Methods in Chemistry, Springer, New York, 1991.
[25] P.L.A. Popelier, Atoms in Molecules-An Introduction, Pearson Edition, Harlow, UK, 1999.
[26] R.F.W. Bader, T.T. Nguyen-Dang, Adv. Quantum. Chem. 14 (1981) 63.
[27] J.P. Perdew, Phys. Rev. B33 (1986) 8822.
[28] M.J. Frisch, G.W. Trucks, H.B. Schlegel, G.E. Scuseria, M.A. Robb, J.R. Cheeseman, J.A. Montgomery Jr., Vreven, K.N. Kudin, J.C. Burant, J.M. Millam, S.S. Iyengar, J. Tomasi, V. Barone, B. Mennucci, M. Cossi, G. Scalmani, N. Rega, G.A. Petersson, H. Nakatsuji, M. Hada, M.P. Ehara, K. Toyota, R. Fukuda, J. Hasegawa, M. Ishida, T. Nakajima, Y. Honda, O. Kitao, H. Nakai, M. Klene, X. Li, J.E. Knox, H.P. Hratchian, J.B. Cross, Adamo, J. Jaramillo, R. Gomperts, R.E. Stratmann, O. Yazyev, A.J. Austin, R. Cammi, C. Pomelli, J.W. Ochterski, P.Y. Ayala, Morokuma, G.A. Voth, P. Salvador, J.J. Dannenberg, V.G. Zakrzewski, S. Dapprich, A.D. Daniels, M.C. Strain, O. Farkas, D.K. Malick, A.D. Rabuck, K. Raghavachari, J.B. Foresman, J.V. Ortiz, Q. Cui, A.G. Baboul, S. Clifford, J. Cioslowski, B.B. Stefanov, G. Liu, A. Liashenko, P. Piskorz, I. Komaromi, R.L. Martin, D.J. Fox, T. Keith, M.A. Al-Laham, C.Y. Peng, A. Nanayakkara, M. Challacombe, P.M.W. Gill, B. Johnson, W. Chen, M.W. Wong, C. Gonzalez, J.A. Pople, Gaussian 03, Revision D.1, Gaussian, Inc., Wallingford, CT, 2005.
[29] J. Cheeseman, T.A. Keith, R.F.W. Bader, AIMPAC Program Package, McMaster University Hamilton, Ontario, 1992.
[30] T.A. Keith, AIMAll (Beta Version 09.08.26), 2009.
[31] T. Koritsanszky, P. Macchi, C. Gatti, L.J. Farrugia, P.R. Mallinson, A. Volkov, T. Richter, XD-2006. A Computer Program Package for Multipole Refinement and Topological Analysis of Charge Densities and Evaluation of Intermolecular Energies from Experimental or Theoretical Structure Factors, Version 5.33, 2007.
[32] C.B. Hubschle, P. Luger, J. Appl. Crystallogr. 39 (2006) 901.
[33] J. Ellena, A.E. Goeta, J.A.K. Howard, G. Punte, J. Phys. Chem. A105 (2001) 8696.
[34] A. Bach, D. Lentz, P. Luger, J. Phys. Chem. A105 (2001) 7405.
[35] D.E. Hibbs, O. Jacob, J.A. Platts, M.P. Waller, M.B. Hursthouse, J. Phys. Chem. B108 (2004) 3663–3672.
[36] E.J. Yearley, E.A. Zhurova, V.V. Zhurova, A. Alan Pinkerton, J. Am. Chem. Soc. 129 (2007) 15013.
[37] K.B. Wiberg, Tetrahedron 24 (1998) 1083.
[38] Y.A. Abramov, L. Brammer, W.T. Klooster, R.M. Bullock, Inorg. Chem. 37 (1998) 6317.
[39] O.Y. Borbulevych, O.V. Shishkin, M.Y. Antipin, J. Phys. Chem. A106 (2002) 8109.
[40] D. Chopra, T.S. Cameron, J.D. Ferrara, T.N. Guru Row, J. Phys. Chem. A110 (2006) 10465.
[41] P.L.A. Popelier, J. Phys. Chem. A102 (1998) 1873–1878.
[42] P. Coppens, Y. Abramov, M. Carducci, B. Korjov, N. Irina, C. Alhambra, M.R. Pressprich, J. Am. Chem. Soc. 121 (1999) 2585.
[43] A. Volkov, P. Coppens, Acta. Crystallogr. A 57 (2001) 395.
[44] P.C. Mishra, A. Kumar, in: J.S. Murray, K.D. Sen (Eds.), Molecular Electrostatic Potentials: Concepts and Applications, Theoretical and Computational Chemistry Book Series, vol. 3, Elsevier, Amsterdam, 1996.
[45] A. Volkov, C. Gatti, Y. Abramov, P. Coppens, Acta. Crystallogr. A56 (2000) 252.
[46] R.S. Mulliken, J. Chem. Phys. 23 (1955) 1833.
[47] A.E. Reed, R.B. Weinstock, F.A. Weinhold, J. Chem. Phys. 83 (1985) 735.
[48] R.F.W. Bader, T.T. Nguyen-Dang, Y. Tal, Rep. Prog. Phys. 44 (1981) 893.
[49] S. Zhang, T.N. Truong, J. Phys. Chem. A104 (2000) 7304.
[50] B.M. Rice, S. Sahu, F.J. Owens, J. Mol. Struct. (Theochem) 583 (2002) 69.
[51] Q. Zhao, S. Zhano, Q.S. Li, Chem. Phys. Lett. 407 (2005) 105.
[52] D. Chakraborty, R.P. Muller, S. Das Gupta, W.A. Goddaod, J. Phys. Chem. A104 (2000) 2261.
[53] P.W. Cooper, Explosive Engineering, Wiley-VCH, USA, 1996.
[54] F.J. Owens, K. Jayasuriya, L. Abrahamsen, P. Politzer, Chem. Phys. Lett. 116 (1985) 434.
[55] J.S. Murray, M.C. Concha, P. Politzer, Mol. Phys. 107 (2009) 89.
[56] A. David Stephen, R.B. Pawar, P. Kumaradhas, Prop. Exp. Pyrotec. (2005), doi:10.1002/prep.2010000f3.
[57] A. David Stephen, R.B. Pawar, P. Kumaradhas, J. Mol. Struct. (Theochem) 959 (2010) 55.
[58] K. Maheswari, A. David Stephen, R.B. Pawar, P. Kumaradhas, unpublished manuscript.
[59] A.B. Felipe, A. Toro-Labbe, unpublished manuscript.
[60] A.B. Felipe, A. Toro-Labbe, T. Brinck, J.S. Murray, P. Politzer, J. Mol. Model. 16 (2010) 1679.